AGU PUBLICATIONS

Geophysical Research Letters

RESEARCH LETTER

10.1002/2015GL066664

Key Points:
- Mars surface radiation is unique and quite different from Earth
- We present the first measurement of the zenith angle dependence
- This has broad implications for exploration and understanding Mars history

Correspondence to:
R. F. Wimmer-Schweingruber,
wimmer@physik.uni-kiel.de

Citation:
Wimmer-Schweingruber, R. F., et al. (2015), On determining the zenith angle dependence of the Martian radiation environment at Gale Crater altitudes, *Geophys. Res. Lett.*, *42*, 10,557–10,564, doi:10.1002/2015GL066664.

Received 20 OCT 2015
Accepted 11 DEC 2015
Accepted article online 15 DEC 2015
Published online 31 DEC 2015

On determining the zenith angle dependence of the Martian radiation environment at Gale Crater altitudes

Robert F. Wimmer-Schweingruber[1], Jan Köhler[1], Donald M. Hassler[2,3], Jingnan Guo[1], Jan-Kristoffer Appel[1], Cary Zeitlin[4], Eckart Böhm[1], Bent Ehresmann[2], Henning Lohf[1], Stephan I. Böttcher[1], Sönke Burmeister[1], Cesar Martin[1], Alexander Kharytonov[1], David E. Brinza[5], Arik Posner[6], Günther Reitz[7], Daniel Matthiä[7], Scott Rafkin[2], Gerald Weigle[8], and Francis Cucinotta[9]

[1]Institute for Experimental and Applied Physics, University of Kiel, Kiel, Germany, [2]Southwest Research Institute, Boulder, Colorado, USA, [3]Institut d'Astrophysique Spatiale, Paris XI-Paris Sud, Orsay, Orsay, France, [4]Lockheed Martin IS and GS, Oakland, California, USA, [5]Jet Propulsion Laboratory, California Institute of Technology, Pasadena, California, USA, [6]NASA HQ, Washington, District of Columbia, USA, [7]Institute of Aerospace Medicine, DLR, Cologne, Germany, [8]Big Head Endian, Burden, Kansas, USA, [9]Department of Health Physics and Diagnostic Services, Las Vegas, Nevada, USA

Abstract We report the zenith angle dependence of the radiation environment at Gale Crater on Mars. This is the first determination of this dependence on another planet than Earth and is important for future human exploration of Mars and understanding radiation effects in the Martian regolith. Within the narrow range of tilt angles ($0 \le \theta_0 \le 15°$) experienced by Curiosity on Mars, we find a dependence $J \propto \cos^{\gamma'}(\theta)$ with $\gamma' = 1.18 \pm 0.07$, which is not too different from an isotropic radiation field and quite different from that at sea level on Earth where $\gamma' \approx 2.0$.

1. Introduction

The galactic cosmic rays (GCR) outside the Martian atmosphere are approximately isotropic with small (<1%) anisotropies, mainly related to the movement of the Sun and observer through the interstellar and interplanetary medium [e.g., *Ahluwahlia and Dessler*, 1962; *Jacklyn*, 1966; *Nagashima et al.*, 1989]. The interaction of the GCR with a planetary atmosphere leads to a change of the isotropic nature of the radiation field which, on Earth, results in a larger directional flux of particles from the zenith than from the horizon. Intuitively, this can be understood as due to shielding by the atmosphere which has a much smaller column density in the zenith direction than toward the horizon. In this work we report the first determination of this zenith angle dependence on the surface of Mars using data from the Radiation Assessment Detector (RAD) [*Hassler et al.*, 2012] which is part of the Mars Science Laboratory (MSL) payload [*Grotzinger et al.*, 2012]. Initial surface measurements are summarized and reported in *Hassler et al.* [2014] and are not discussed further here.

An isotropic distribution as present in interplanetary space is described by equation (1). In such a distribution the number of particles incident on a spherical detector is the same from every infinitesimal solid angle, $d\Omega = \sin(\theta) d\theta d\phi$. Here θ is the angle measured from the zenith, and ϕ is the azimuthal angle. Including the projection onto a zenith-pointing plane detector of unit area, the thus normalized counts are given by

$$dn = d\Omega \cos(\theta)\, dA = \cos(\theta)\, \sin(\theta)\, d\theta\, d\phi\, dA, \quad (1)$$

where dA is the differential area of the detector and $\cos(\theta)$ accounts for the projection effect [*Sullivan*, 1971].

The angular dependence of the directional flux on Earth [*Grieder*, 2001] is often given as

$$J(\theta, \phi) \propto \cos^{\gamma'} \theta, \text{ where } \gamma' \approx 2. \quad (2)$$

This way of presenting the zenith angle dependence is somewhat misleading because it implicitly contains the geometric projection effect by assuming that the detector is zenith pointing, i.e., its detection plane is horizontal. Because the RAD on Curiosity does not always point exactly toward zenith, the effect of atmospheric shielding and geometric projection are better treated separately. Therefore, we state the zenith angle dependence of radiation as

$$J(\theta) \propto \cos(\theta') \cdot \cos^{\gamma}(\theta), \quad (3)$$

where the projection effect is explicitly split out as a separate $\cos\theta'$ term and θ' only equals θ for a zenith-pointing detector. Here $\gamma = 0$ would correspond to an isotropic radiation field (equation (1)) and $\gamma = 1$ to that observed at sea level on Earth, equation (2).

As primary GCR particles enter the atmosphere they interact with its nuclei via multiple processes [*Grieder*, 2001], many of which ionize the atmosphere or produce secondary particles which in turn also lead to ionization. *Pfotzer* [1936a, 1936b] found that the ionization of the Earth's atmosphere reached a maximum (today called the Pfotzer maximum) at an altitude of about 20 km, corresponding to a column density often cited as $\sim$100 g/cm^2 [e.g., *Grieder*, 2001], not too different from recent measurements in a high-altitude balloon which showed a maximum of the count rate in Si at 64 ± 3 g/cm^2 [*Möller et al.*, 2013]. The thin Martian atmosphere at Gale crater only provides approximately 21 g/cm^2 shielding [*Rafkin et al.*, 2014]. Consequently, on the Earth's surface, we are below, and at Gale crater on Mars, Curiosity is above the Pfotzer maximum. This underlines how different the Martian surface radiation environment is from that on the Earth's surface [*Hassler et al.*, 2014], and the need for an accurate characterization thereof. We expect the zenith angle dependence of the Mars surface radiation to be quite different from that measured on Earth but possibly close to isotropic due to the only very light shielding provided by the Martian atmosphere. We also note that, different from Earth, Mars has no global magnetic field [*Smith et al.*, 1965; *Acuna et al.*, 1998] which would provide further shielding from the GCR. As discussed in section 2, we have essentially only one model variable to adjust to our measurements and therefore only one parameter with which to parametrize a radiation model. Therefore, generalizing observations on Earth [*Grieder*, 2001], we model it as the power law dependence given in equation (3), where the exponent, γ, is unknown but of obvious importance for understanding the radiation environment on Mars.

We describe RAD and the geometry of the measurements in section 2 and our data analysis in section 3. Results are presented in section 4 and discussed in section 5.

2. The Radiation Assessment Detector

The Radiation Assessment Detector (RAD) is a very compact and versatile instrument which was optimized for operation on Mars [*Hassler et al.*, 2012] to asses the charged and neutral particle radiation environment. A simplified cross section of RAD is shown in Figure 1. The A Si solid-state detector has two segments, A1 and A2, which together with the B detector form two fields of view (FoV) indicated by short and long dashed lines in Figure 1. Because segment A1 is larger, the FoV spanned by it has a larger geometric factor, $\sim$0.73 cm^2 sr, than that spanned by A2, $\sim$0.17 cm^2 sr, for an isotropic radiation field. The opening angles are α_1=32.4°and α_2 = 19.9°.

RAD is mounted inside Curiosity such that its FoV points along the normal to the rover deck. Thus, the inclination of RAD is the same as that of the rover. Its inclination angle, θ_0, was obtained from the Mars Science Laboratory SPICE kernel using spiceminer (http://github.com/et-uni-kiel/spiceminer/). The azimuthal rotation angle, θ_0, is irrelevant for our purposes.

RAD generates a large number of data products [*Hassler et al.*, 2012] including so-called Pulse-Height-Analysis (PHA) words in which the full information of a measurement is recorded. A subset of these PHA words is sent to Earth via telemetry together with a number of counters which allow us to reconstruct the observations on Mars, albeit with larger statistical uncertainties. In this work we used all PHA words which recorded a coincidence between B and A1 or B and A2. Using PHA words allowed us to use cuts in the data to minimize possible background, e.g., from scattered electrons mainly due to Curiosity's radiothermal generator (RTG), or also due to electronic cross talk. A minimally ionizing particle deposits approximately 100 keV in the A or B detectors. We required the energy deposition in A1 or A2 to be larger than 30 keV and larger than half the signal seen in B and less than twice the signal seen in B. To avoid possible cross talk, we also required that the signal in A2 be less than 10 keV to ensure that a particle passed through A1, and vice versa for particles passing through A2.

The geometric factors, $g_{A1} \approx 0.73$ cm^2 sr and $g_{A2} \approx 0.17$ cm^2 sr given in *Hassler et al.* [2012] were calculated for an isotropic radiation field and using the approximation of circular detectors of the same area. The ratio of counts in A1 and A2 depends on the ratio of the respective geometry factors and on the exact zenith angle distribution and thus differs for different values of the $\cos^\gamma\theta$ index, γ. We calculated the count ratios for A1·B and A2·B coincidences for $\cos\theta$ indices $\gamma \in \{-1.5, -1.4, \ldots, 0.0, \ldots, 2.0\}$ and for inclination angles $\theta_0 \in \{0, 1, \ldots, 24, 25\}$ degrees. The integration was performed by triangulating the hexagonal RAD detectors with 384 equilateral triangles, yielding g_{A1}=71.535 $\pm$ 9.5 $\cdot$ 10^{-3} mm^2 sr and g_{A2}=17.025 $\pm$ 1.4 $\cdot$ 10^{-3} mm^2 sr,

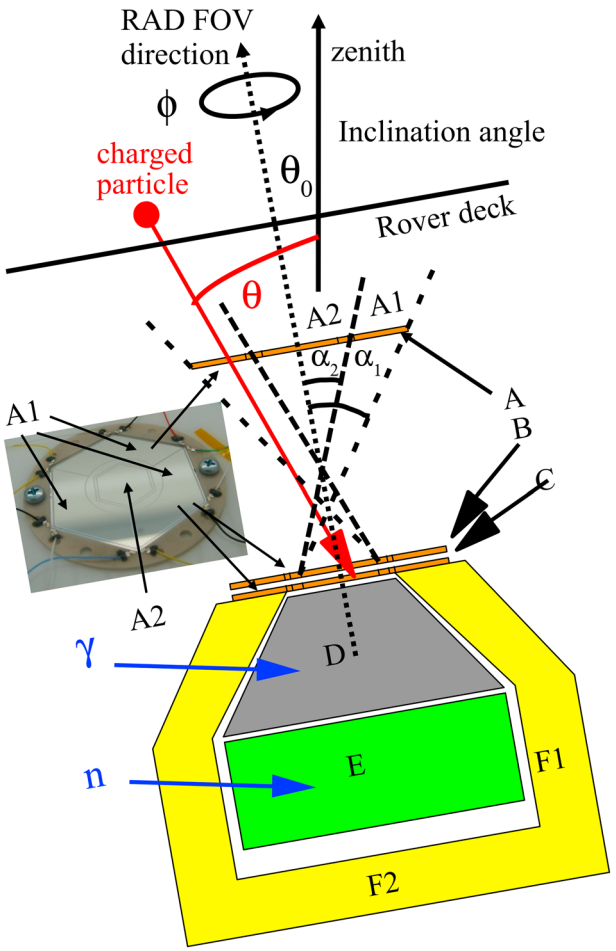

Figure 1. RAD consists of three solid-state detectors (A, B, and C) forming a particle telescope, a Tl-doped CsI scintillator crystal functioning as a calorimeter, and a (tissue-equivalent) plastic scintillator (E). D and E are enclosed in an efficient anti coincidence (F1 and F2) which is closed by detector C in the upward direction. Detector A has two concentric segments, A1 (outer) and A2 (inner), as can be seen in the photographic insert and is indicated by vertical lines in the sketch.

respectively, for the isotropic case ($\gamma = 0$). These values for the A1 and A2 geometry factors differ slightly from the values given in *Hassler et al.* [2012] for the aforementioned reason. The errors given are the difference between this calculation using 384 triangles and a finer triangulation using 3750 triangles.

3. Data Analysis

RAD instrument settings were optimized multiple times after landing. For this study we used hourly data from sol 525 to sol 806 when no changes were made to the RAD configuration. Sols are Martian days after landing on Mars on 6 August 2012. In the time period investigated, RAD observed one solar energetic particle (SEP) event on sol 737. Count rates increased by less than 25%, and it only lasted approximately half a sol, so we did not exclude it from our analysis. However, we disregarded all RAD observations which could have been contaminated by active Dynamic Albedo of Neutrons (DAN) measurements using the corresponding time tags. DAN, the Dynamic Albedo of Neutrons instrument [*Mitrofanov et al.*, 2012] uses intense pulses of 14.1 MeV neutrons to detect subsurface water. These neutrons interact with the various RAD detectors and are clearly seen in RAD data if not filtered out. Because count rates depend on the temperature in the detector front-end electronics (an instrumental effect), RAD adjusts its thresholds according to temperature. RAD operates autonomously and alternates between a "SLEEP" mode and "SCIENCE" observations. When booting, RAD measures the temperature and chooses the appropriate temperature table. Temperatures ranged from ~10°C to nearly 40°C, the temperature tables were carefully adjusted to ensure that the temperature-dependent noise peak does not contribute to science counts. Four different temperature tables were in use during the time period investigated here.

The path traveled by Curiosity during this time period resulted in the distribution of inclination angles, θ_0, shown in Figure 2 (bottom). They varied between 0 and 15°, the most probable value was 6.5°, the mean and median were 5.8 and 6°, respectively. The small variation in θ_0 together with the much larger RAD field of view results in a very small change in the count rate which is completely masked by other effects such as pressure-dependent shielding, secondary production, and heliospheric modulation.

Mars atmospheric pressure is measured by the Rover Environmental Monitoring Station (REMS) instrument [*Gómez-Elvira et al.*, 2012]. REMS pressure measurements for the time period investigated here are shown in Figure 2 (top). Pressure varied between approximately 680 Pa to about 930 Pa over the period chosen for this study. The wideband in Figure 2 shows the magnitude of the diurnal pressure variations. The pressure and RAD observations often take place at different times; we therefore interpolated the actual pressure measurements for every single RAD observation. These pressure values are the ones shown in Figure 2. *Rafkin et al.* [2014]

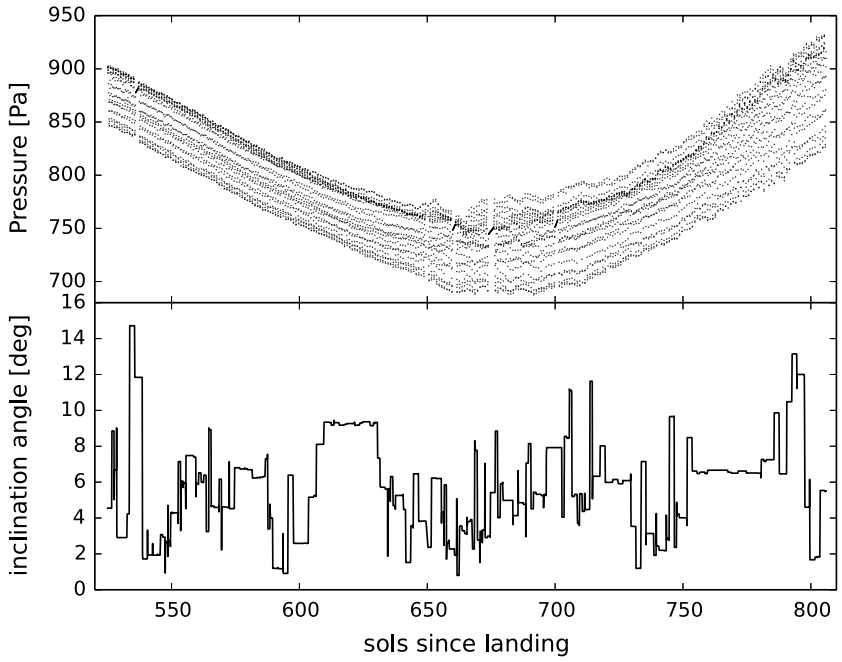

Figure 2. (top) Pressure and (bottom) inclination angle versus time between sols 525 and 806.

reported diurnal variations in dose rate measured by RAD which are due to pressure variations and which completely mask the minute θ_0 dependence of the count rate.

We explain the data analysis using the A1·B coincidence measurements as an example. The same steps were performed for A2·B and other needed data. Since we cannot send to Earth every single PHA word, the number of (e.g., priority-1, see *Hassler et al.* [2012]) PHA words has to be scaled using the appropriate (i.e., priority-1) counters. For every observation we know not only the number of A1·B coincidence PHA words but also the number of priority 1 PHA words and can scale them accordingly (see *Hassler et al.* [2012] for details). As mentioned above, we have three quantities which can potentially affect our measurements: temperature, inclination angle, and pressure.

In order not to mask possible dependences, we binned all measurements into a four-dimensional space (pressure, p, inclination angle, θ_0, temperature, and temperature table). We then divided the accumulated and priority-corrected A1·B counts by the A2·B counts for every point in $\theta_0 - p$ space. This count ratio is determined by the ratio of the A1 and A2 geometry and the zenith angle dependence of the radiation as discussed in section 2. The result is shown in Figure 3. Figure 3 (top right) shows the count ratio plotted versus inclination angle, θ_0, (y axis) and pressure, p, (x axis). The data were accumulated over all temperatures and temperature tables for this plot. It is obvious that we do not have a complete coverage in the $\theta_0 - p$ space. This is the result of variations in the attitude of the rover and the diurnal and seasonal pressure variations. This panel shows no clear trend, some bins show higher and some show lower count rates, but this is expected and compatible with the error estimates for each individual bin. Figure 3 (top left) shows the pressure-averaged ratio versus inclination angle; Figure 3 (bottom) the inclination-angle-averaged data versus pressure. No significant trend can be seen in the averaged data (Figure 3, top left and bottom), an observation that was borne out by fitting a plane to the data in Figure 3 (top right). The shaded area in Figure 3 (top left and bottom) gives the 95% confidence level for the expectation value given by this fit; error bars are standard deviations for individual data point and reflect the uneven counting statistics for each point.

4. Results and Interpretation

The ratio of counts shown in Figure 3 is independent of pressure and inclination angle, θ_0, as just stated and as expected. While the dose rate in B does depend on pressure [*Rafkin et al.*, 2014], the fact that we use a ratio of counts cancels out this dependence. The average value obtained by fitting a plane to the data was 4.18 ± 0.05. To assess the statistical robustness of this result, we computed additional estimates for the "central" value

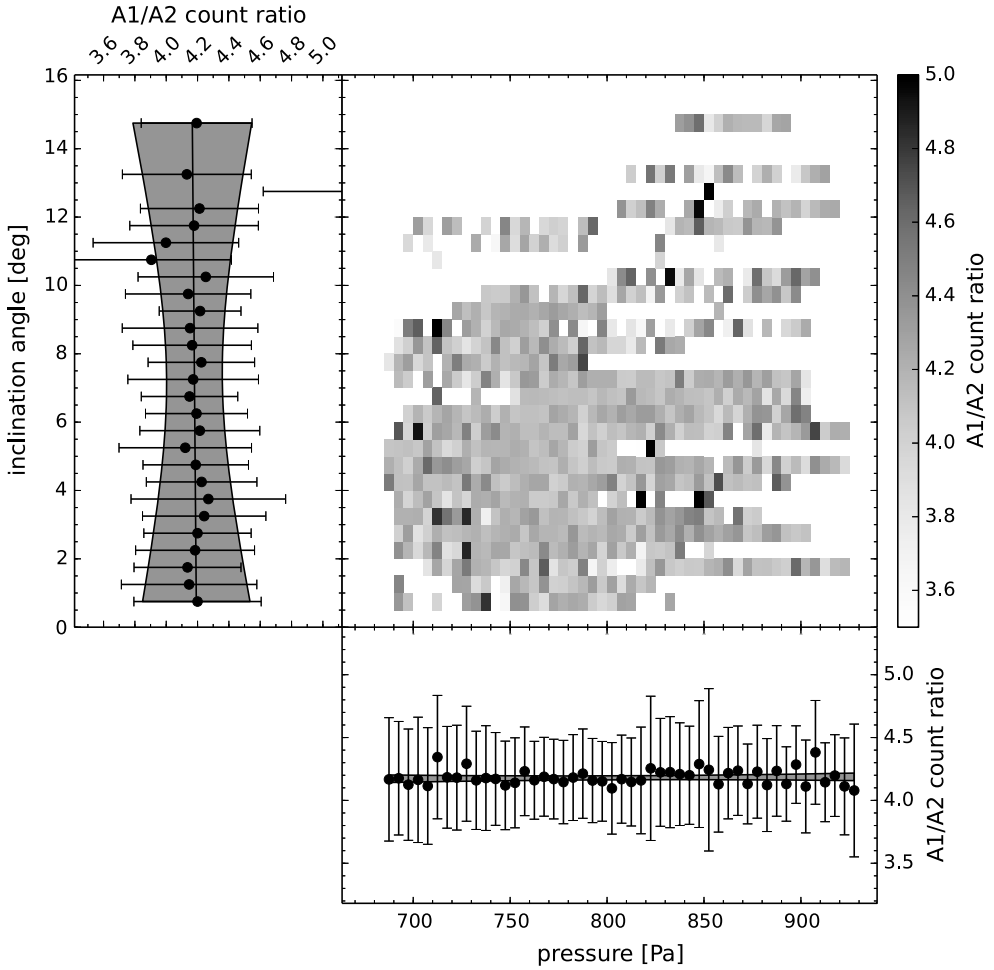

Figure 3. (top right) Grey shade coded ratio of A1·B/A2·B counts as a function of inclination angle, θ_0 (y axis) and pressure p (x axis). (top left) Projected (summed over all pressure bins) count ratio versus inclination angle, θ_0. (bottom) Projected (summed over all pressure bins) count ratio versus pressure, p. No systematic trend can be seen in the data.

of this quantity. We plot a histogram of the values for the count ratio in Figure 4. The solid curves show fits of a Gaussian and a Lorentzian (as indicated by arrows) to the well-peaked histogram. Obviously, it is better represented by a Lorentzian than a Gaussian. The dashed line gives the cumulative sum of the data, the dotted and dash-dotted line those of the Gaussian and Lorentzian fits. The results are summarized in Table 1.

Taking the unweighted average of the values given in Table 1, we find our final value for the count ratio A1·B / A2·B, i.e., $A1/A2_{\mathrm{Mars}} = 4.173 \pm 0.012$. This needs to be compared to the value obtained for an isotropic radiation field, $A1/A2_{\mathrm{iso}} = 4.202 \pm 6.6 \times 10^{-4}$. Thus, $A1/A2_{\mathrm{Mars}}$ differs from the isotropic case, $A1/A2_{\mathrm{iso}}$, by 2.4 times the estimated error. Where not stated differently, error estimates were obtained using the standard Gaussian error propagation throughout this work. Assuming underlying Gaussian errors, the chance that we are truly observing an isotropic distribution is 1.6%. As one sees in Figure 4, an underlying Lorentzian error distribution more closely resembles the data. Using this assumption and the corresponding fitted width of the distribution given in Table 1, we obtain a probability of ~10% for an isotropic distribution "masquerading" as nonisotropic. Given these uncertainties, we may state that the radiation field coming from within zenith angles of up to ~15° at Gale crater is very close to isotropic and tends to show added shielding from larger zenith angles.

The results presented in Table 1 can be used to estimate the $\cos\theta$ index, γ. Taking the values for the modeled ratio for A1·B and A2·B coincidences (described in section 2), we can interpolate in them to find the index, γ,

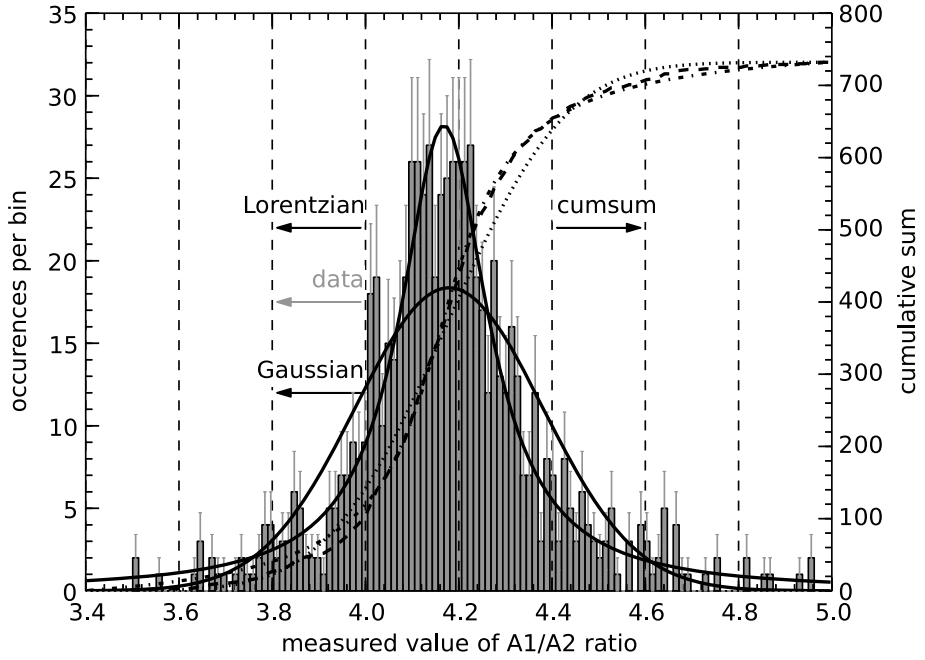

Figure 4. Histogram of the values of the count ratio (grey bars) and fits of a Gaussian and Lorentzian centroid estimator (indicated by arrows). The cumulative sum of the data is given as a dashed line, the dotted and (barely visible) dash-dotted lines give the cumulative sums of the Gaussian and Lorentzian, respectively.

corresponding to $A1/A2_{\mathrm{Mars}} = 4.173 \pm 0.012$. We thus found $\gamma_{\mathrm{Mars}} = 0.18 \pm 0.07$. As expected from the discussion in the previous paragraph, this is not too different from the isotropic value $\gamma_{\mathrm{iso}} \doteq 0$ and indicates that the very thin Martian atmosphere provides only a small amount of shielding or that the shielding effect is partially compensated by the generation of secondary particles from the interaction of the GCR with the atmosphere. Indeed, our model described in section 2 shows that we must not expect a measurable dependence of the A1/A2 ratio on the inclination angle, θ_0, for this value of γ, which is consistent with our observation that it indeed does not vary with θ_0.

For the γ_{Mars} derived in this work, the average incidence angle for a zenith-pointing RAD is 10.1° for A2 and 18.9 degrees for A1. In other words, the two fields of view see a different average column density, which is easily computed. As one may readily convince oneself, the column density, ρ_c, in a barometric atmosphere varies with pressure as $\rho_c = p/g$, where p is pressure and g is the (Martian) gravitational acceleration at Mars surface. As can be seen in Figure 2, pressure varied between 680 Pa and 940 Pa during the time period investigated here. The average value was 793 Pa, the median 784 Pa, and the most probable value 770 Pa. Inserting $p = 780$ Pa as a typical value and using $g = 3.711$ m/s^2, we obtain an average column density of $\rho_c \approx 21$ g/cm^2. Thus, the average column densities for A1 and A2 are approximately 22.2 g/cm^2 and 21.3 g/cm^2, respectively. In other words, the shielding by the atmosphere is about 4% larger for A1 than for A2 but so is the atmospheric target for secondary particle generation.

That the shielding effect is small can be understood with the following simple considerations. Taking typical bounding values for the pressure variations of $p_{\mathrm{lo}} \approx 700$ Pa and $p_{\mathrm{hi}} \approx 900$ Pa, we get $\rho_{c\,\mathrm{lo}} \approx 19$ g/cm^2 and $\rho_{c\,\mathrm{hi}} \approx 24$ g/cm^2, both values lie well above the Pfotzer maximum which lies at $\rho_{c\,\mathrm{Pf}} \approx 64$ g/cm^2 [*Möller et al.*, 2013]. The primary energy needed by a proton to penetrate 19 g/cm^2 of carbon dioxide (a good approximation for the Martian atmosphere) is about 155 MeV (see http://physics.nist.gov/PhysRefData/Star/). For the most probable value of 21 g/cm^2 it is about 165 MeV, and for the typical upper limit, $\rho_{c\,\mathrm{hi}} \approx 24$ g/cm^2, it is about 178 MeV. The spectrum of GCR protons is broad and peaks at several hundred MeV [*Grieder*, 2001] and the fraction of GCR protons affected by this shielding is minute. We estimated the removal of incident protons due to this variable shielding to be less than 1% using the Planetocosmics [*Desorgher et al.*, 2006] input spectrum.

Table 1. Best Estimates for the Values of the A1/A2 Count Ratio

Quantity	Value	Error
Mean[a]	4.186	0.009
Weighted average[b]	4.171	0.006
Median	4.169	–
Most probable value	4.175	–
Gaussian centroid	4.173	0.018
Lorentzian centroid	4.162	0.010

[a]Equal weights for every value.
[b]With inverse errors as weights.

The generation of secondary particles is also not strongly affected by the 4% increase in atmospheric column density. The mean free path for high-energy protons ($E_{kin} > 1$ GeV, i.e., the majority of GCR protons) is given by

$$\lambda = \frac{1}{n\sigma}; \quad \sigma \approx 4 \times 10^{-26} A^{2/3} \mathrm{cm}^2; \quad n = \rho \cdot N_A / A, \tag{4}$$

where N_A is Avogadro's number, ρ density, and A the atomic mass number. This evaluates to $\lambda \approx A^{1/3} 41.5$ g/cm$^2/\rho$ or approximately 100 g/cm$^2/\rho$. Thus, Gale Crater at typically 21 g/cm^2 lies at a height where only few reactions have had a chance to take place. The difference of 4% in column density then results in a difference of less than 1% in the number of reactions which could produce secondary charged particles.

Together, the shielding and secondary particle production nearly cancel, with shielding apparently being slightly more important, to result in the $\gamma_{Mars} = 0.18 \pm 0.07$ given above.

5. Discussion and Conclusions

We have shown that the radiation coming from within some 15° from the zenith direction at Gale Crater on Mars is nearly isotropic and that shielding plays only a minor role in this range of zenith angles. Seasonal and diurnal pressure variations do not influence the A1/A2 count ratio. While limited to a rather narrow range of zenith angles, this finding has implications for future human exploration of Mars and for investigations of the interaction of radiation with the Martian soil. We have not yet compared our observations with model results, but we expect that they will serve as an important observational constraint on the modeling of charged-particle transport through the Martian and other planetary atmospheres.

It is important to note that these observations were only made in a rather narrow range of zenith angles and our finding of a nearly isotropic radiation field should not be extrapolated to larger zenith angles. In future work, we will attempt to extend this range by adding newer data from RAD when Curiosity began climbing Mount Sharp and experienced somewhat higher inclination angles. This will require careful calibration of temperature effects and other possible configurations changes to RAD.

Despite these restrictions our results can be generalized to other locations at Mars, at least for altitudes corresponding to the pressure range seen during this investigation.

Acknowledgments
RAD is supported by NASA (HEOMD) under JPL subcontract 1273039 to Southwest Research Institute and in Germany by DLR and DLR's Space Administration grant 50QM0501 and 50 QM1201 to the Christian Albrechts University, Kiel. Part of this research was carried out at the Jet Propulsion Laboratory, California Institute of Technology, under a contract with the National Aeronautics and Space Administration. In particular, we would like to extend sincere gratitude to Jeff Simmonds, Ashwin Vasavada, and Joy Crisp at JPL, Gale Allen, Michael Meyer, Chris Moore, Victoria Friedensen at NASA HQ, and Heiner Witte at DLR in Germany for their unwavering support of RAD over the years. This research has made use of NASA's Astrophysics Data System. The data used in this paper may be retrieved from the NASA Planetary Data System.

References

Acuna, M. H., et al. (1998), Magnetic field and plasma observations at Mars: Initial results of the Mars Global Surveyor Mission, *Science*, *279*, 1676, doi:10.1126/science.279.5357.1676.

Ahluwahlia, H. S., and A. J. Dessler (1962), Diurnal variation of cosmic radiation intensity produced by a solar wind, *Planet. Space Sci.*, *9*, 195–210, doi:10.1016/0032-0633(62)90148-4.

Desorgher, L., E. O. Flückiger, and M. Gurtner (2006), The PLANETOCOSMICS Geant4 application, paper presented at 36th COSPAR Scientific Assembly, vol. 2361, COSPAR Meeting, Beijing.

Gómez-Elvira, J., et al. (2012), REMS: The environmental sensor suite for the Mars Science Laboratory rover, *Space Sci. Rev.*, *170*, 583–640, doi:10.1007/s11214-012-9921-1.

Grieder, P. K. F. (2001), *Cosmic Rays at Earth*, Elsevier Science, Switzerland.

Grotzinger, J. P., et al. (2012), Mars Science Laboratory mission and science investigation, *Space Sci. Rev.*, *170*, 5–56, doi:10.1007/s11214-012-9892-2.

Hassler, D. M., et al. (2012), The Radiation Assessment Detector (RAD) investigation, *Space Sci. Rev.*, *170*, 503–558, doi:10.1007/s11214-012-9913-1.

Hassler, D. M., et al. (2014), Mars surface radiation environment measured with the Mars Science Laboratory's Curiosity rover, *Science*, *343*(6169), 1244797, doi:10.1126/science.1244797.

Jacklyn, R. M. (1966), Evidence for a two-way sidereal anisotropy in the charged primary cosmic radiation, *Nature*, *211*, 690–693, doi:10.1038/211690a0.

Mitrofanov, I. G., et al. (2012), Dynamic Albedo of Neutrons (DAN) experiment onboard NASA's Mars Science Laboratory, *Space Sci. Rev.*, *170*, 559–582, doi:10.1007/s11214-012-9924-y.

Möller, T., B. Ehresmann, J. Labrenz, and L. Panitzsch (2013), Radiation measurements on the stratospheric balloon BEXUS 13, ESA Special Publ., 21st ESA Symposium on European Rocket and Balloon Programmes and Related Research, pp. 637–640, Noordwijk, Netherlands, doi:10.13140/2.1.4096.2565.

Nagashima, K., K. Fujimoto, S. Sakakibara, Z. Fujii, and H. Ueno (1989), Galactic cosmic-ray anisotropy and its modulation in the heliomagnetosphere, inferred from air shower observation at Mt. Norikura, *Nuovo Cimento C Geophys. Space Phys. C*, *12*, 695–749, doi:10.1007/BF02511970.

Pfotzer, G. (1936a), Dreifachkoinzidenzen der Ultrastrahlung aus vertikaler Richtung in der Stratosphäre, *Z. Physik*, *102*, 23–40, doi:10.1007/BF01336829.

Pfotzer, G. (1936b), Dreifachkoinzidenzen der Ultrastrahlung aus vertikaler Richtung in der Stratosphäre, *Z. Physik*, *102*, 41–58, doi:10.1007/BF01336830.

Rafkin, S. C. R., et al. (2014), Diurnal variations of energetic particle radiation at the surface of Mars as observed by the Mars Science Laboratory Radiation Assessment Detector, *J. Geophys. Res.*, *119*, 1345–1358, doi:10.1002/2013JE004525.

Smith, E. J., L. Davis Jr., P. J. Coleman Jr., and D. E. Jones (1965), Magnetic field measurements near Mars, *Science*, *149*, 1241–1242, doi:10.1126/science.149.3689.1241.

Sullivan, J. D. (1971), Geometrical factor and directional response of single and multi-element particle telescopes, *Nucl. Instrum. Meth.*, *95*, 5–11.